Bioelectrochemistry 128 (2019) 39–48

Contents lists available at ScienceDirect

Bioelectrochemistry

journal homepage: www.elsevier.com/locate/bioelechem

Interpretation of the electrochemical response of a multi-population biofilm in a microfluidic microbial fuel cell using a comprehensive model

Mohammad Mahdi Mardanpour *, Maryam Saadatmand, Soheila Yaghmaei

Department of Chemical and Petroleum Engineering, Sharif University of Technology, Tehran, Iran

ARTICLE INFO

Article history:
Received 29 December 2018
Received in revised form 22 February 2019
Accepted 12 March 2019
Available online 16 March 2019

Keywords:
Microfluidic
Biosensor
Modeling
Multi-population
Biofilm

ABSTRACT

The present study investigates the diversification and dynamic behavior of a multi-population microfluidic microbial fuel cell (MFC) as a biosensor. The cost effective microfluidic MFC coupled to a comprehensive model, presents a novel platform for monitoring chemical and biological phenomena. The importance of competition among different microbial groups, hierarchical biochemical processes, bacterial chemotaxis and different mechanisms of electron transfer were significant considerations in the present model. The validation of the model using experimental data from a microfluidic MFC shows an appropriate match with the hierarchal biodegradation processes of a complex substrate as well as development of bacterial chemotaxis during multi-population biofilm formation under real conditions. Microfluidic MFC performance, including temporal and spatial distribution of different microbial group concentrations in the biofilm and anolyte bulk, the competitive behavior of different species, bacterial transport parameters and bioelectrochemical characteristics are also assessed.

1. Introduction

Microfluidic technology utilizing small scale fluid volumes is defined on the basis of three physical concepts, including laminar flow, surface and interfacial tension and capillary forces. The microbial fuel cell (MFC) as a bioelectrochemical system deriving electrical current using microorganisms can be considered to operate on dimensional scales of micro, *meso* and macro, respectively [1]. Microscale MFCs or microfluidic MFCs (MMFCs) are regarded as a MFC where anolyte volume is lower than 200 μl [2]. Provision of a high-surface area, low-cost, controllability, and facility for integration into a single system are the main features of microfluidic MFCs, allowing manipulation and real-time monitoring of generated power [1].

Once the characteristic length of the anolyte chamber is reduced to millimeter scale, viscous effects and surface forces become critical to microfluidic flow [2]. Generally, micro-sized MFCs are categorized into two groups, including ml-scale MFCs (with an anolyte volume of 1 to 7 ml) and μl-scale MFCs (with an anolyte volume of 1 to 200 μl) [3].

In the Lam et al. (2006) study, the microfluidic MFC was described as photosynthetic electrochemical. The maximum produced 1.1 μA cm^{-2} current density in the microfluidic MFC was obtained. The cell was composed of a 50 μl volume for each anodic and cathodic chamber [4]. The further studies on the microfluidic MFC by the cell elements modification, specially their electrodes showed more current density in the lower anodic volume. Chen et al. achieved the maximum current density of 214.8 μA cm^{-2} in a 25-μL microfluidic MFC. The cell was fabricated by the photolithography technique and equipped with modified plate-shaped gold anodic electrode [5]. The modification of microfluidic MFCs' structure to prevent oxygen permeability can obtain more power density even in lower volumes. Yoon et al. developed a polydimethylsiloxane based co-laminar microfluidic MFC utilizing a parylene C coating and micropillar-structured gold electrode as the anode. The anodic chamber volume was equal to 0.3 μl and the maximum current density of 182 μA cm^{-2} was obtained [6].

The microfluidic MFC applications as a novel amperometric biosensor such as assessment of water quality [7,8], measuring dissolved oxygen [9], evaluation of biochemical oxygen demand (BOD) [10], sensing DNA [11], and monitoring volatile fatty acids in anaerobic digestion process [12–14] were reported in previous studies. Regard to the MFCs performance, the generated current is an instrumental characteristic of the biological/biochemical processes progresses to predict bacterial distribution status and substrate degradation [15–17].

The ability of micro-sized systems to quantify the free-swimming bacterial cells' motion and associated characteristics in microbial multi-population dynamics, biofilm formation and dispersion reveals new horizon for pursuit of future researches [1,2,18]. In addition, the quantification of substrates degradation rates illustrates the microfluidic MFCs as the powerful biosensors for monitoring both chemical and biological characteristics of different industrial systems [19].

In biological monitoring view point and owning to the experimental methods limitations, the critical role of modeling to predict the free-

* Corresponding author.
E-mail address: mardanpourm@ripi.ir (M.M. Mardanpour).

https://doi.org/10.1016/j.bioelechem.2019.03.003
1567-5394/

swimming bacterial cell dispersions, diversifications, interactions, and the intermediate compounds production at each step of the complex substrate biodegradation is inevitable [17,20,21].

Among various biological processes, based on the usage prevalence, the biodegradation monitoring processes of a complex substrate in anaerobic biological systems is one of critical issues [14,22,23]. The hierarchical biochemical processes of anaerobic digestion engaged by different microorganisms are initiated by a hydrolysis of big biopolymer molecules to hydrolysates. The conversion of hydrolysates to simple organic acids by acidogens, the simple organic acids conversion to acetate, carbon dioxide hydrogen by acetogens and finally, the produced acetate/hydrogen conversion to electrons by electrogens and/or to methane by acetoclastic or hydrogenotrophic methanogens are the other steps of substrate biodegradation nominated as anaerobic digestion process [24]. Fig. S1 shows these hierarchical biochemical processes of anaerobic digestion in Supplementary Material.

The inability to sense the diversification and dynamic microbial population behaviors during the biodegradation process was the main deficiency of most previous MFCs' models [25,26]. As in previous studies [27,28], the microfluidic MFC applications to analyze bioelectrochemical processes that were engaged with pure cultures were investigated, to date there is no performed study about dynamical analysis of multi-population MFCs as a biosensor to characterize the microbial diversification. In addition, the both chemical and biological phenomena investigation in the macroscale MFCs are associated with the numerous assumptions and inaccuracies. The microfluidic techniques and associated models have paved the way for better understanding of the biological complex reactions and it is incorporating and monitoring capability in the real-time response of multiple cell types interacting in a system [29]. The controllable anolyte flow in the microchannel mimics the real behavior of substrate degradation at the anolyte bulk and biofilm interfaces in compared to the conventional macroscale MFCs.

In regard with previous multi-population models deficiency in macroscale MFCs, the initial bacteria distribution on the electrode's surface was assumed and its suitability was assessed, based on the predicted results matching with the experimental data of the current density evolutions [26] and/or polarization curves [25]. The next generation of microbial groups developed based on this initial distribution. Therefore, the competition role among different microorganism groups in initial and sustained microbial distributions was disregarded.

This study demonstrates the novel model as an auxiliary tool coupled to the cost-effective microfluidic MFC for monitoring chemical and biological phenomena. The simulation of multi-population biofilm formation by engaging more comprehensive processes of bacterial chemotaxis that could not be explained conclusively in macro systems were investigated. The current study is the first novel model on microfluidic MFC that have the prominent monitoring feature and investigate the microbial competition, complex substrates degradation as well as the mechanisms of free-swimming microorganisms' dispersion in anolyte bulk and/or their attachment to electrode's surfaces to extend the multi-population biofilm.

2. Materials and methods

2.1. Model configuration

In order to investigate the behavior of free-swimming multi-population cells and the biofilm formation dynamics, this study used a mathematical description of multi-population bacterial distribution and various biochemical processes in both anolyte and biofilm by a combination of Anaerobic Digestion Model (ADM1) [24,25] and bacterial chemotaxis as well as different electron transfer mechanisms. Table 1 described the summarized governing equations of this model as well as their initial and boundary conditions. The definition of each parameter, details about equations terms and the boundary conditions description are presented in Supplementary Material.

The governing equations were divided into three main parts including microorganism's distribution, substrates distribution and electron generation for both anolyte and biofilm. The microorganisms and substrates distributions denoted for i microbial group (including sugar (Su), amino acids (Aa), fatty acids (Fa), propionate (Pro), and C4 (including butyrate (But), and valerate (Val)) consuming microbes as well as acetoclastic methanogens (AM), hydrogenotrophic methanogens (HM), and electrogens (El)) at spatial position z and time t.

The different microorganisms' enrollment as biocatalysts in the hierarchical biochemical reactions of complex substrates degradation was achieved in the form of suspended species in the anolyte and/or attached species to the electrode surface as biofilm. The motion of different microorganisms through the anolyte bulk and their recruitment to the pioneering colonies depends on the secreted sensing molecules production [30]. The first row of Table 1 shows the mass balance of secreted sensing molecules.

Table 1
The summarized governing equations of present model (the details are presented in Supplementary Material).

		Equation	Initial and Boundary Conditions	Ref.
Microorganisms Distribution	Secreted Molecules	$\frac{\partial C_{E,i}}{\partial t} = D_{E,i}\frac{\partial^2 C_{E,i}}{\partial z^2} - \lambda_i C_{E,i} + \alpha_i \psi_{s,i}$ $(Bacteria\ Species\ (i) = Su, Aa, Fa, Pro, C_4, E, AM, HM)$	$C_{E,i}\vert_{t=0} = C_{E,i0}, D_{E,i}\frac{\partial C_{E,i}}{\partial z}\vert_{z=L_f} = \omega_i \psi_{a,i}$, $\frac{\partial C_{E,i}}{\partial z}\vert_{z=0} = 0$	[30]
	Anolyte	$\frac{\partial \psi_{s,i}}{\partial t} = \mu_{SE0,i}\frac{\partial^2 \psi_{s,i}}{\partial z^2} - \chi_{S0,i}\frac{\partial}{\partial z}(\psi_{s,i}\frac{\partial C_{E,i}}{\partial z}) + \Gamma_{i,anolyte}$ $(Bacteria\ Species\ (i) = Su, Aa, Fa, Pro, C_4, E, AM, HM)$	$\psi_{s,i}\vert_{z=0} = 0, \frac{\partial \psi_{s,i}}{\partial z}\vert_{z=H_{micro}} = 0$, $\psi_{s,i}\vert_{t=0} = \psi_{s,i0}$	[30]
	Biofilm	$\frac{\partial \psi_{a,i}}{\partial t} = \mu_i \frac{\partial^2 \psi_{a,i}}{\partial z^2} - \frac{\partial}{\partial z}(V_i \psi_{a,i}) + \Gamma_{i,biofilm}$ $(Bacteria\ Species\ (i) = Su, Aa, Fa, Pro, C_4, E, AM, HM)$	$\frac{\partial \psi_{a,i}}{\partial z}\vert_{z=0}, \frac{\partial \psi_{a,i}}{\partial z}\vert_{z=L_{f,i}} = 0, \psi_{a,i}\vert_{t=0} = l^*$	[31]
Substrates Distribution	Anolyte	$\frac{\partial C_{i',bulk}}{\partial t} = -U_{i',bulk}, i' = Charbohydrates, Proteins, Lipids$ $(\frac{\partial C_{i,bulk}}{\partial t}) = D(C_{i,in} - C_{i,bulk}) - (\sum \Lambda)_{i,bulk}$	$C_{i,bulk}\vert_{t=0} = C^0_{i,bulk}$ $(Bacteria\ Species\ (i) = Su, Aa, Fa, Pro, C_4, E, AM, HM)$	[28]
	Biofilm	$D_{s,f,i}\frac{\partial^2 C_{i,biofilm}}{\partial z^2} + (\sum \Lambda)_{i,biofilm} = 0$ $(Bacteria\ Species\ (i) = Su, Aa, Fa, Pro, C_4, E, AM, HM)$	$\frac{\partial C_{i,biofilm}}{\partial z}\vert_{z=0} = 0$ $D_{s,f,i}\frac{dC_{i,biofilm}}{dz}\vert_{z=L_f} = (\frac{D_{s,l,i}}{L})(C_{i,bulk} - C_{i,surface})$	[25]
Electron Generation	Anolyte	$\frac{dM_{ox}}{dt} = -\gamma_M U_{El,\ max} + \frac{M_{Med} \times I_{MFC} \times 86.4}{V_{micro} \times \psi_{s,El} \times nF}$ $I_{MFC} = \frac{1}{R_{ext}}(E_{Theoretical} - \frac{RT}{\delta nF}\ \sinh^{-1}(\frac{I_{MFC}}{A_{an} i_0}) - I_{MFC} R_{int} - \frac{RT}{nF}\ \ln(\frac{M_{Total}}{M_{red}}))$	$M_{ox}\vert_{t=0} = M^0_{ox}$	[26]

The microorganisms distribution including temporal and spatial variations in the biofilm and anolyte bulk of microfluidic MFC based on the microorganisms flux to electrodes surface that be characterized by Keller–Segel (K–S) model (the second row of Table 1) [31,32], and the swimming of cells toward the concentration bands of secreted sensing molecules [30] (the third row of Table 1).

The temporal different substrates variation (which is indexed by i) in anolyte bulk is described by the substrates' convection in the bulk solution minus degradation rate of substrates by suspended microorganisms and substrates' diffusion to the biofilm (the forth row of Table 1). Moreover, the different substrates spatial distribution in biofilm is based on its diffusion into the porous solid biofilm (which is shown in the fifth row of Table 1). It should be noted that the boundary conditions of different substrates distribution equations were written as no substrate flux at the anode surface, and an interphase mass transfer at the biofilm/liquid bulk interface.

Finally, to consider electron production in the both biofilm and anolyte, the electricity generation is calculated as transferred electron summation by suspended electrogens convection (via electron shuttles such as cytochrome C as shown in the sixth row of Table 1) and attached electrogens conduction (via nanowires as shown in the seventh row of Table 1). It is also worth noting that cytochromes also play an important role in electron transfer based on nanowires, and the mechanisms of direct and indirect electron transfer [33,34]. The produced electron of suspended microorganisms was described based on the temporal variation of oxidized form of electron shuttles (M_{ox}) that is equal to summation of mediator generation by electrogens and oxidized form reduction of mediator as function of produced current (I_{MFC}) and suspended electrogens concentration ($\Psi_{s,El}$). In addition, microfluidic MFC overpotentials including activation (η_{Act}), ohmic (η_{Ohm}), and concentration (η_{Con}) overpotentials were considered in present model that decrease theoretical cell potential. The produced electron conduction by attached microorganisms is presented by the electrons generated by substrate consumption $\frac{F\gamma_1}{\tau} f_e^0 U_{Ac,El,biofilm}$ and the endogenous respiration $\frac{F\gamma_2}{\tau} r_{res}$ [35].

It should be noted that other supplementary equations including the substrate biodegradation rate, microorganisms' deactivation and respiration of active microorganisms as well as numerical methods description and equations constants are contained in Supplementary Material.

2.2. Model assumptions

The temperature and pH of the system were assumed to be well controlled and biological inhibition were not considered in this model. Moreover, a one-dimensional distribution of substrates and microbial groups in the biofilm and anolyte was another assumption of the current model that could not be considered in macro system. The maximum substrates uptake rate of different tangent planes in the microchannel is assumed to be consistent. It should be noted that due to the big size of biopolymer molecules, the hydrolysis process mainly considers in the anolyte of the microfluidic MFC.

3. Results and discussion

3.1. Model verification

The numerical methods for solving partial differential equations and the presented model validation by the experimental data from synthetic wastewater fed microfluidic MFC in different injection rates. Fig. 1 shows the design of the microfluidic MFC [27]. The microfluidic MFC consists of a single microchannel (1 mm in depth; 1 mm in width; 8 cm in length) that was cut by a laser beam as an anodic compartment. A nickel plate anode (0.5 mm in thickness; 1 mm in width; 5 cm in length) was glued to one side of the anodic compartment and the carbon cloth cathode (5 cm in length and 3 mm in width) was placed in front of the nickel. Variable external resistance (1–100 kΩ) was used to polarize the cell and monitor current variation.

Based on the urine wastewater composition [36], the prepared synthetic wastewater contained 1.36 g l^{-1} $NaCH_3COO.3H_2O$, 0.74 g l^{-1} KCl, 0.8 g l^{-1} creatinine ($C_4H_7N_3O$), 0.5 g l^{-1} urea (H_2NCONH_2), 0.1 g l^{-1} glucose ($C_6H_{12}O_6$), 0.58 g l^{-1} NaCl, 0.68 g l^{-1} KH_2PO_4, 0.87 g l^{-1} K_2HPO_4, 0.28 g l^{-1} NH_4Cl, 0.1 g l^{-1} $MgSO_4.7H_2O$, and 0.1 g l^{-1} $CaCl_2.2H_2O$.

The synthetic wastewater had a 1000 mg l^{-1} COD. Table S15 shows the general parameters used in the microfluidic MFC simulation in Supplementary Material. The activated sludge was obtained from the second sedimentary tank of domestic wastewater treatment, Tehran, Iran and used as the inoculums. The culture was injected in the microfluidic MFC in the total concentration of 8 $kgCOD_X$ m^{-3} in conjunction with the synthetic wastewater. To verify the presented model with the experimental data, Table S17 shows the initial substrates composition and the related organic compounds in the synthetic wastewater.

As shown in Fig. 2, the appropriate matching of the model prediction results and the experimental data indicates a consistency of hierarchal biochemical processes engaged with multi-population biocatalysts in complex substrate biodegradation [26] as well as bacterial chemotaxis foundation for biofilm formation with real conditions [28].

The presented model was analyzed based on the microfluidic MFC characteristics in Sections 3.2 to 3.4. Similar to synthetic wastewater composition, the equivalent composition of organic feed for analysis the model results were speculated as follow: 20 $mgCOD_s$ l^{-1} lipids,

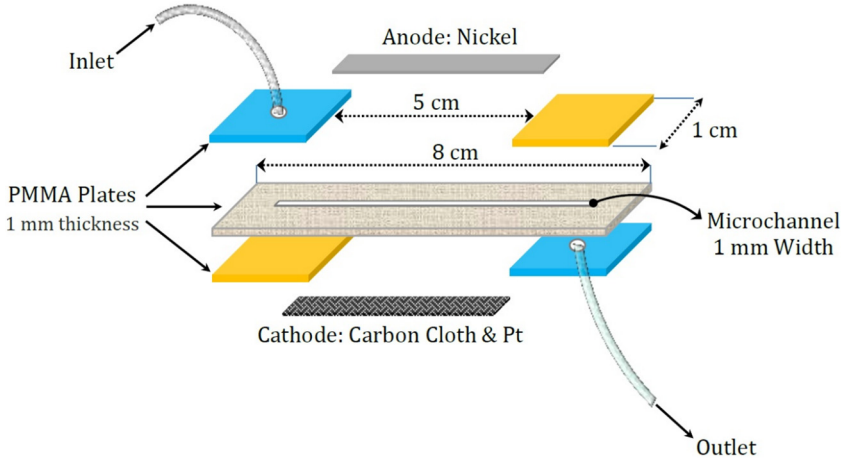

Fig. 1. Schematic of microfluidic MFC [27].

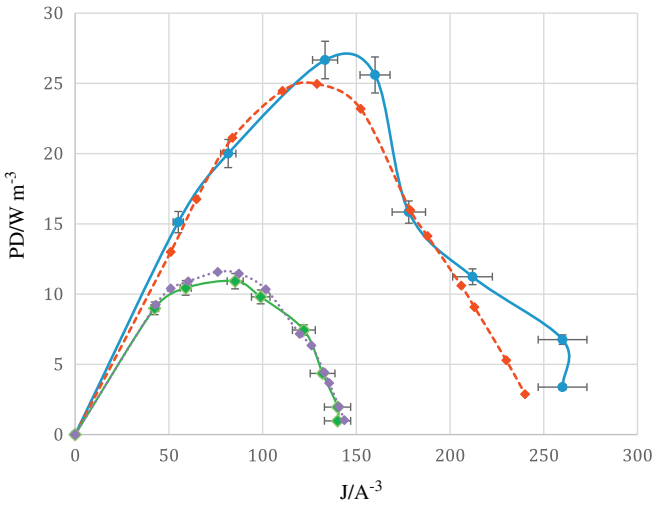

Fig. 2. Model verification with experimental data for urine wastewater fed microfluidic MFC in different injection rates of substrate (experimental results in 100 μl h^{-1} (●) and 1 ml h^{-1} (◆), model predictions in 100 μl h^{-1} (■) and 1 ml h^{-1} (▲)). External resistances of 100, 60, 30, 10, 2, 1 kΩ were used experimentally to obtain power density curves.

100 $mgCOD_s$ l^{-1} proteins, 20 $mgCOD_s$ l^{-1} carbohydrates, 20 $mgCOD_s$ l^{-1} long chain fatty acids (LCFAs), 100 $mgCOD_s$ l^{-1} sugar, 20 $mgCOD_s$ l^{-1} amino acids, 20 $mgCOD_s$ l^{-1} propionate, 20 $mgCOD_s$ l^{-1} butyrate, 20 $mgCOD_s$ l^{-1} valerate, 900 $mgCOD_s$ l^{-1} acetate, 3 $mgCOD_s$ l^{-1} methane and 3 $mgCOD_s$ l^{-1} proton.

3.2. The substrates and microorganisms' distribution in the biofilm

The temporal and spatial distribution of substrates and different microbial group concentrations in the microfluidic MFC that could not be measured easily by experimental methods are the first results of the presented model (Figs. 3 and 4).

Fig. 3 shows the temporal and spatial distribution of substrate concentration in the biofilm of microfluidic MFC. In this figure, each subfigure comprises a set of the lines and each line represents the temporal substrate concentration variation in one step size of microchannel height.

As can be seen in Fig. 3A, the concentration of sugar was decreased abruptly after 10 h of cell operation and then increased negligibly along the concentration of sugar-consuming microbes as shown in Fig. 4A. In addition, it can be inferred from Fig. 4A that the maximum biofilm thickness of sugar-consuming microbes was about 8 μm after 50 h of microfluidic MFC operation.

Fig. 3B shows a significant increasing enhancement in the amino acids' concentration in compare to fatty acids and sugar. This may have contributed to an excess proteins' concentration in fresh feed that hydrolysis to amino acids by hydrolatic microorganisms.

Fatty acids (with concentration variation of 0.015 $mgCOD_s$ cm^{-3}) have the lowest concentration variation in porous biofilm (Fig. 3C). Since same concentrations of fatty acids, amino acids, propionate, valerate and butyrate were considered in fresh feed of microfluidic MFC, fatty acids had a low share in the acidogenesis processes and acetogenesis. Besides, the lowest growth of fatty acids-consuming microbes among other microbial groups (about 0.008 $gCOD_x$ cm^{-3}) confirms this aspect (Fig. 4C).

As shown in Fig. S1 in Supplementary Material, the alteration in valerate/butyrate concentration depends on the acidogenesis rate and acetogenesis processes. Therefore, as shown in Fig. 3E, the reduction of both valerate and butyrate concentrations is related to the acetogenesis process to produce acetate.

The acetate concentration variation which is shown in Fig. 3F is an obvious evidence of triggering the hierarchal biodegradation processes and competition between electrogens and methanogens. An increase in acetate concentration from 900 to 1500 $gCOD_s$ cm^{-3} during 10 h of microfluidic MFC operation is the consequence of a biodegradation processes of complex substrate that produce acetate after hydrolysis, acidogenesis and acetogenesis processes. The descending phase of temporal distribution of acetate concentration is related to an uptake of acetate by both electrogens and acetoclastic methanogens.

Fig. 3 has another significant point that is the abrupt variation in the temporal distribution of all substrate concentrations (that appear in time range of 10 to 15 h of cell operation). It can be observed in Fig. 4 that this is attributed to a significant increase in the attached bacteria concentration. Although this figure shows an ascending trends for all microbial groups, the competition among each microbial group is characterized by the related substrate concentration distribution [25]. Since the competition among microbial groups is a strong function of the net growth rate of microorganisms [37], bacterial transport parameters [38] and substrate accessibility [39], for the same concentration of ingredients in complex substrate, the dynamic substrate concentration variation is an appropriate feature for disclosing the microbial species predominance.

Fig. 4F shows that electrogens with concentration of 130 $gCOD_x$ cm^{-3} have the highest growth among other microbial groups in the microfluidic MFC biofilm. For all microbial groups, the temporal distributions of bacteria concentration revealed an ascending trend. The bacterial aggregations evolution during microfluidic MFC operation is the result of net bacterial growth and bacterial movement as a response to quorum sensing to population density by secreting signaling molecules and/or detachment from biofilm.

The ascending trends of spatial distribution of acidogens concentrations (including sugar-consuming, amino acids-consuming, and fatty acids-consuming microbes which is shown in Fig. 4A, B and C, respectively), and electrogens concentrations (Fig. 4F) from an anode surface ($Z = 0$) to the interphase of the anolyte/biofilm indicate better accessibility for the nutrients in the anolyte/biofilm interphase or the lower thickness of the porous biofilm that expedites substrate diffusion [40,41].

In contrast to acidogens and electrogens, the acetogens concentration (including propionate-consuming and valerate/butyrate-consuming microbes which is shown in Fig. 4E and D, respectively), and methanogens (Fig. 5A and B) have a reverse trend; their concentrations decrease from the anode surface to the interphase of anolyte/biofilm. As shown in Fig. 3D and E, when expected to decrease near the electrode surface, the spatial propionate distribution, and valerate/butyrate concentrations in the biofilm had no sensible variations. This can be attributed to the progress of hierarchical biochemical processes that compensate the concentration reduction in these intermediate substrates. Providing sufficient accessibility to nutrient at the electrode surface as well as the ascending trend of temporal distributions of acetogens and methanogens may facilitate the acetogens increasing and methanogens concentrations in the lower layer of the biofilm. This subject corresponds to experimental investigation [42] and similar modeling prediction data in macro systems [25] which confirms the methanogens existence around electrode surfaces due to low oxygen diffusion.

Fig. S3 shows the temporal and spatial distribution of suspended microorganisms in the anolyte bulk of the microfluidic MFC in Supplementary Material. The variation of suspended bacteria concentrations is negligible in compared to the attached bacteria concentrations. This may be attributed to the bacteria concentrations reduction in the anolyte due to the bacterial attachment to biofilm (as a function of concentration gradient of the secreted sensing molecules [43]) compensated by their net growth.

Fig. 5 shows the temporal and spatial distribution of methanogens and the related substrates concentration in the microfluidic MFC biofilm. Similar to acetogenesis microorganisms, a reverse trend of methanogen concentrations in the biofilm (which is shown in Fig. 5A and B) indicates an increasing in the related substrate concentrations

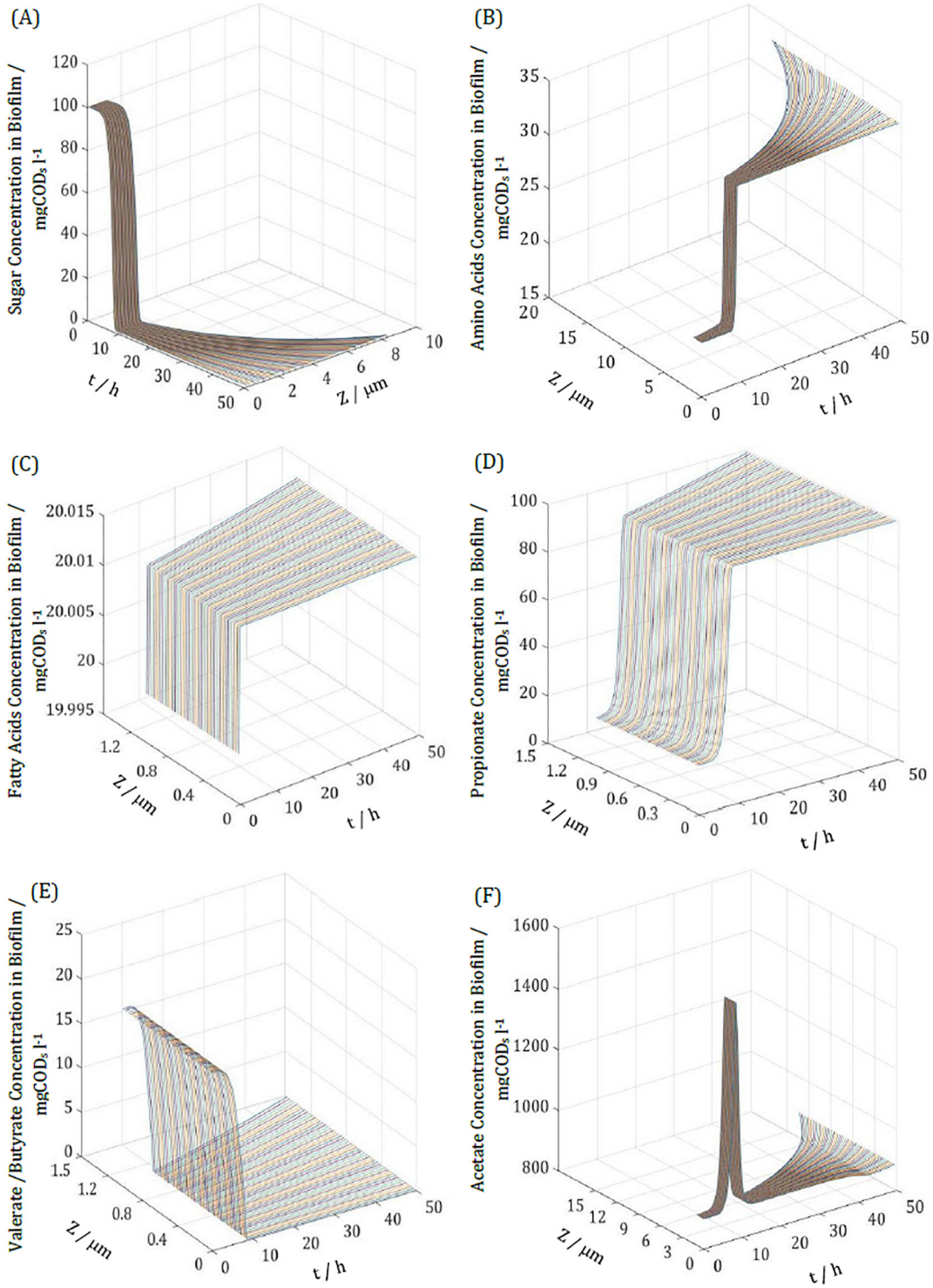

Fig. 3. The temporal and spatial distribution of each substrate concentration (including (A) sugar, (B) amino acids, (C) Fatty acids, (D) propionate, (E) valerate/butyrate, and (F) acetate) in the biofilm of microfluidic MFC. The microchannel diameter, the substrate flow rate and the external resistance were 1000 μm, 100 μl h^{-1} and 30 kΩ, respectively.

(including acetate and proton) in the lower layer of the biofilm. With regard to this subject, Fig. 5E and F show the both methane and proton concentrations reach to more than 5000 and 55 $mgCOD_s$ l^{-1} in microfluidic MFC biofilm, respectively.

It should be noted that the variation of bacteria concentration in anolyte are negligible (that is shown in Fig. 5C and D). The temporal acetoclastic methanogens increasing in the lower thickness of its biofilm (Fig. 5A) is equivalent to the temporal increase in the acetate concentration (Fig. 3F).

3.3. Biofilm formation

Fig. 6 shows the evolution of biofilm thickness of different microbial species. Amino acids-consuming microbes, electrogens, sugar-consuming microbes and hydrogenotrophic methanogens have remarkable growth and/or higher attachment rate to electrode surface in compared to other microbes. The three-dimensional chart of biofilms thickness in Fig. 6C makes a good comparison of the biofilm thickness of each microbial group versus the operating time of the microfluidic MFC.

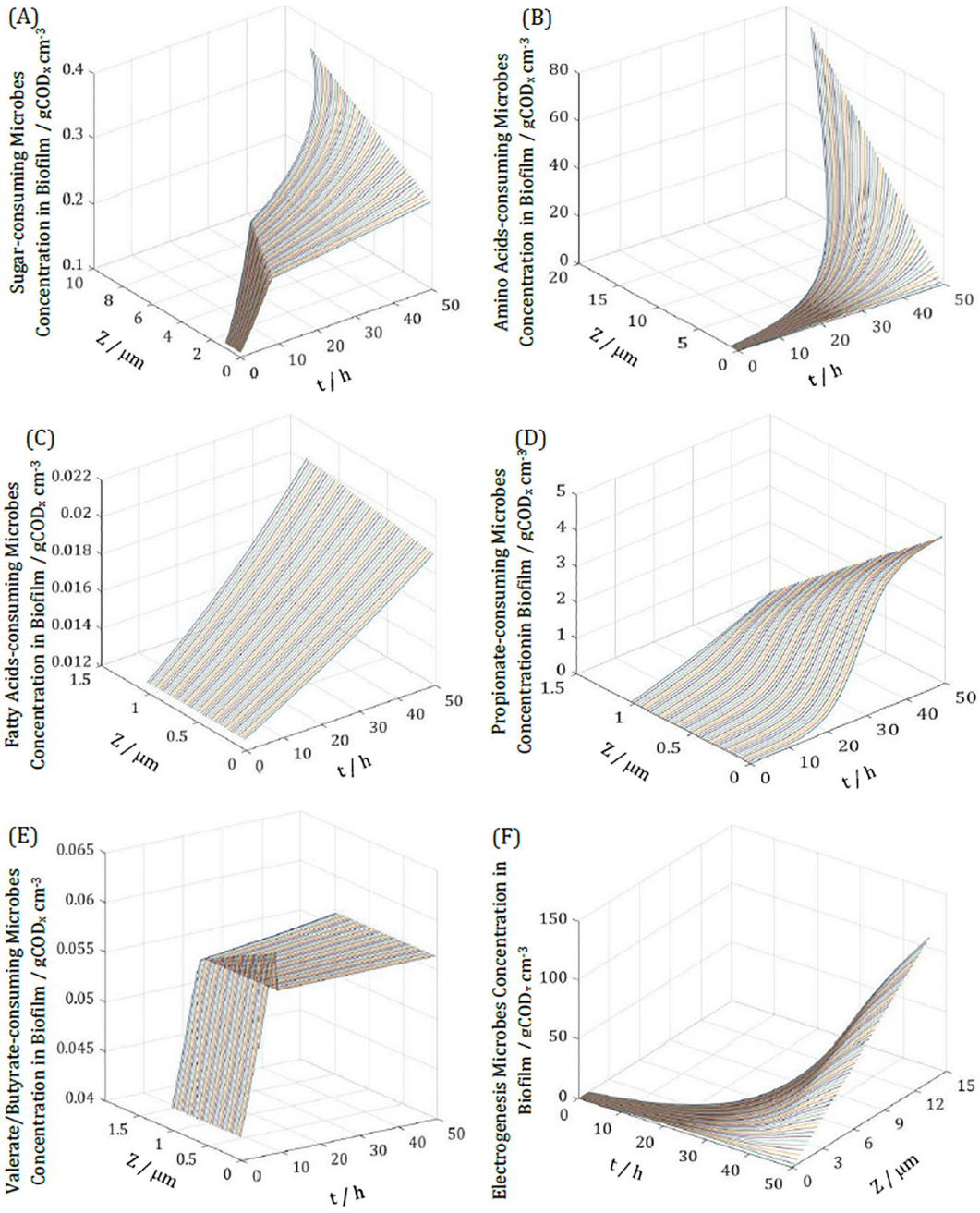

Fig. 4. The temporal and spatial distribution of each bacterial group concentrations (including (A) sugar-consuming, (B)amino acids-consuming, (C) fatty acids-consuming, (D) propionate-consuming, (E) valerate/butyrate-consuming, (F) electrogenesis microbes) in the biofilm of microfluidic MFC. The microchannel diameter, the substrate flow rate and the external resistance were 1000 μm, 100 μl h^{-1} and 30 kΩ, respectively.

Fig. 6C shows a comparison of the biofilm thickness of each microbial group versus the operating time of the microfluidic MFC. At start-up time of microfluidic MFC, the thickness of each species was the same and after 50 h, the existence of amino acid-consuming microbes, electrogens and sugar-consuming microbes was considerable. As mentioned, the significant growth of amino acid-consuming microbes may be attributed to a higher proteins' concentration in fresh feed. However, more experimental data are needed to interpret the effect of protein concentration on the growth of amino acids-consuming microbes.

It should be noted that the temporal variation of chemotactic velocity of each microbial group for urine fed microfluidic MFC is shown in Fig. 4S. As chemotactic velocity increasing leads to shorter time span for the aggregation of bacterial cells to form biomass, the ascending trend of chemotaxis velocity of amino acids-consuming microbes, and electrogens can be ascribed to the priority of these bacteria for biofilm formation. Moreover, the significant growth of these species in compared to others (Fig. 4B and F) is a consequence of higher chemotactic velocities.

3.4. Effect of external resistance on bacterial distribution

Fig. 7 shows the effect of external resistance on the temporal distribution of microbial group concentrations in anolyte and microfluidic MFC biofilm.

The variation of bacteria concentrations versus external resistance to amino acid-consuming microbes, electrogens, sugar-consuming microbes and hydrogenotrophic methanogens are sensible in biofilm in

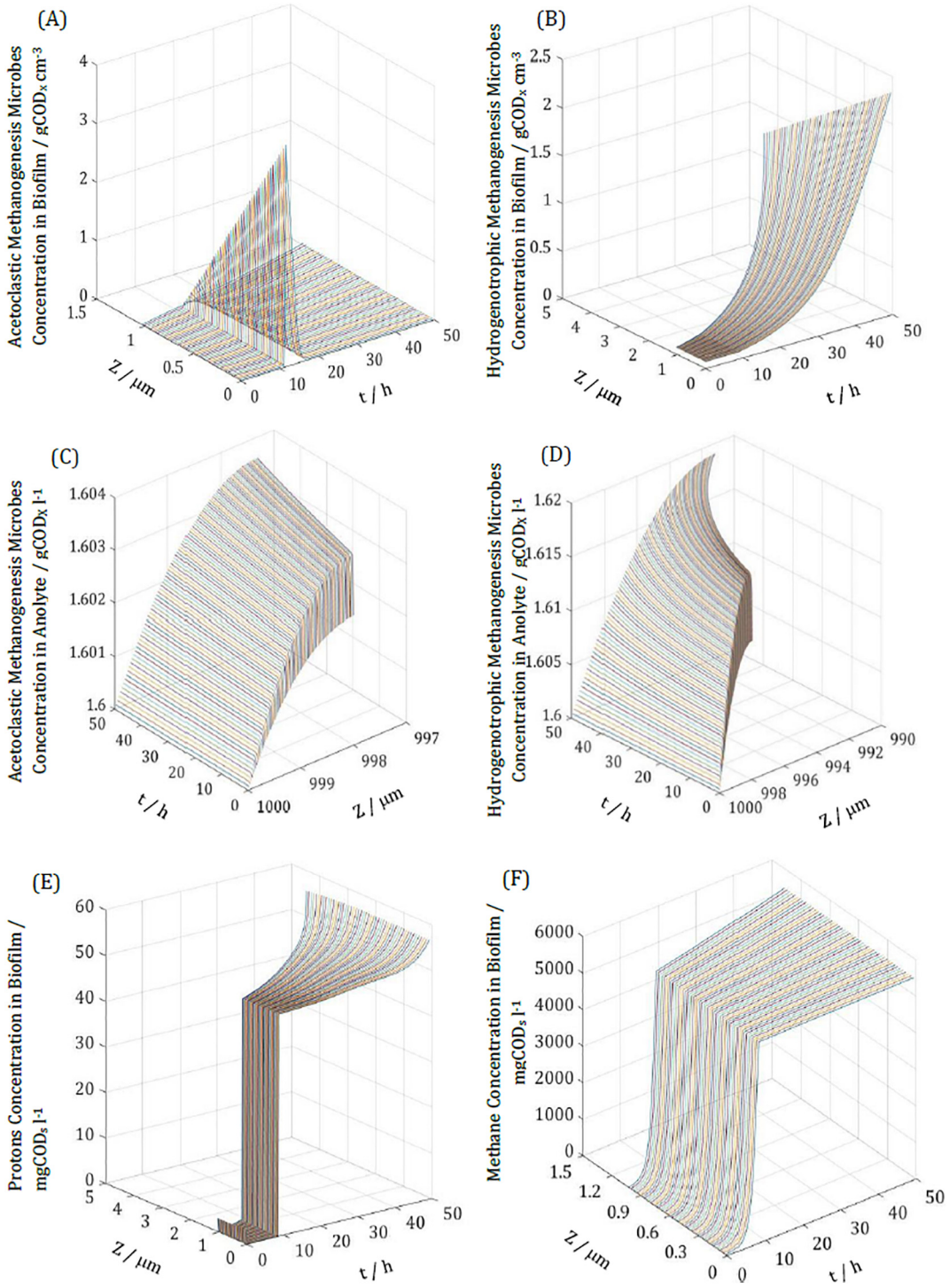

Fig. 5. The temporal and spatial distribution of methanogens and related substrates concentrations: (A) acetoclastic methanogens, (B) hydrogenotrophic methanogens, (C) protons and (D) methane in the biofilm of microfluidic MFC. The microchannel diameter, the substrate flow rate and the external resistance were 1000 μm, 100 μl h^{-1} and 30 kΩ, respectively.

compare to other species or even their values in anolyte of microfluidic MFC.

It can be inferred from Fig. 7 that in the lower external resistance, the bacteria concentration increasing in biofilm for most species is more than under higher external resistance. A large amount of electron transfer accompanies the increasing electrogen concentration, a decrease in external resistance, creates a more conductive path in biofilm matrix, promoting electron shuttles in anolytes. These results have been shown in previous studies on microfluidic MFC inoculated with electrogens [27].

Evidently, the electrogens growth and consequently a great biodegradation of acetate due to decreasing external resistance, precede the rate of hierarchical biochemical processes of other substrate biodegradation. Therefore, the biochemical reaction accelerated by amino acids-consuming microbes and hydrogenotrophic methanogens as biocatalysts have remarkable bacterial growth.

As can be seen in Fig. 7B, decreasing the external resistance did not increase the bacteria concentrations in anolyte, significantly. This can be attributed to a crucial role of biofilm in which a decreasing of external resistance increases the electron transfer path in biofilm in compare to

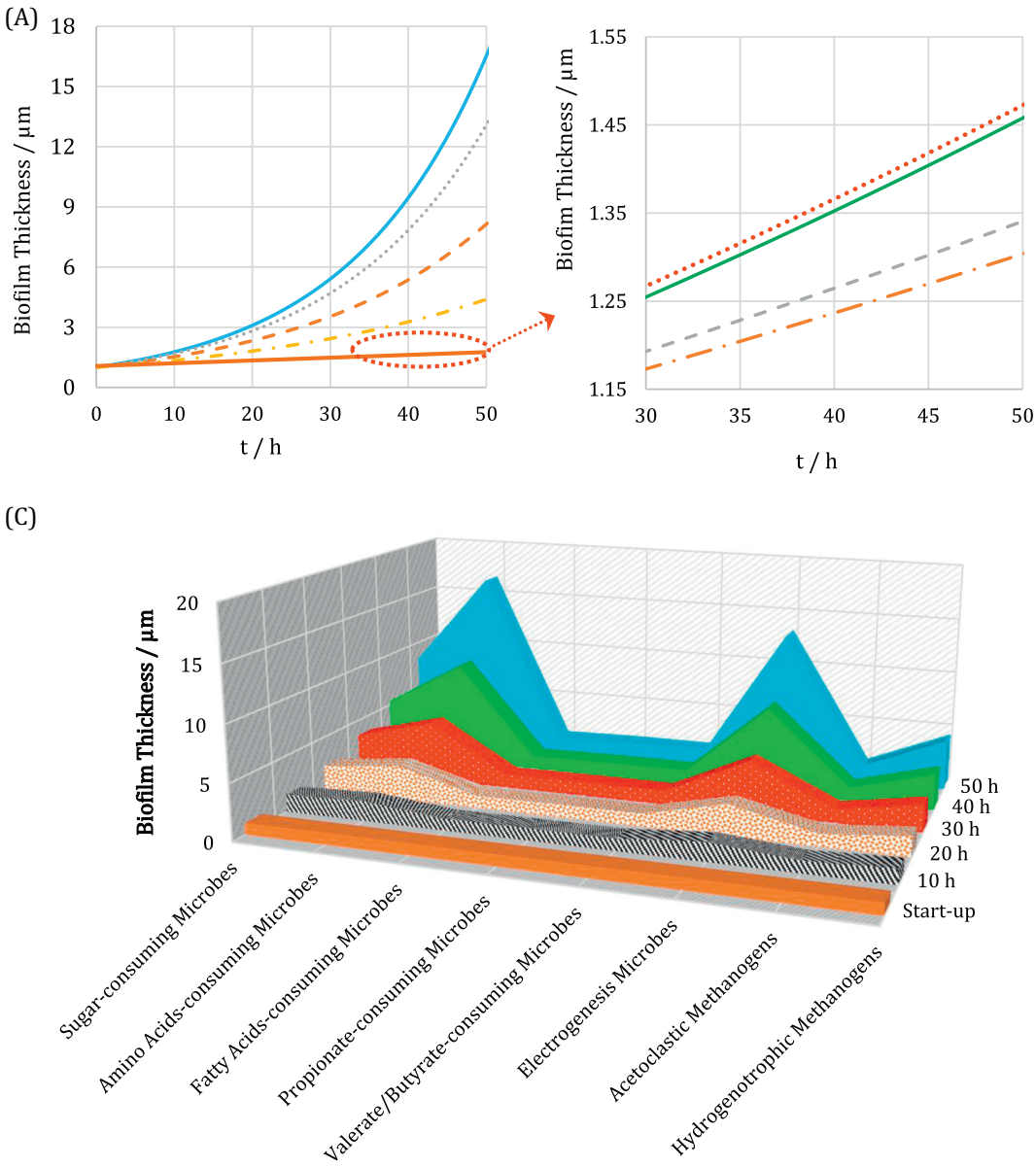

Fig. 6. The biofilm thickness of each microbial group. The microchannel diameter, the substrate flow rate and the external resistance were 1000 µm, 100 µl h^{-1} and 30 kΩ, respectively.

anolyte. For sugar-consuming, amino acid-consuming and valerate/butyrate-consuming microbes, the bacteria concentrations in anolyte from external resistance of 100 kohm to 60 kohm increased significantly. This suggests that the most bacterial groups' concentration in a suspended state reaches the maximum in an external resistance of 60 kohm. In the microfluidic MFC biofilm, the maximum concentration of attached microorganisms was obtained in external resistance of 10 kohm.

4. Conclusion

The performance of multi-population microfluidic MFC fed with complex substrate is assessed based on competition among different microbial groups, bacterial chemotaxis, and bioelectrochemical responses.

The dynamic biofilm formation investigations show a significant increase in attached bacteria concentration that leads to the abrupt variation in the temporal distributions of all substrate concentrations. The spatial distribution of acidogens and electrogen concentrations indicate their aggregation in the anolyte/biofilm interphase. In contrast, the spatial distributions of acetogen and methanogen concentrations demonstrate an ascending trend in the lower layers of biofilm.

Amino acids-consuming microbes, electrogens, sugar-consuming microbes and hydrogenotrophic methanogens have a remarkable growth and/or a higher attachment rate to the electrode surfaces in compare to other microbes. The effect of external resistance on urine-fed microfluidic MFC shows that the concentration of most bacterial groups in a suspended form and biofilm reach the maximum under an external resistance of 60 and 10 kohm, respectively. The electrogens growth and an increased biodegradation of acetate by decreasing external resistance precede the rate of hierarchical biochemical processes of other substrate biodegradation, particularly biochemical reactions accelerated by amino acid-consuming microbes and hydrogenotrophic methanogens as biocatalysts.

The three-dimensional modeling of multi-population microfluidic MFC and engaging computational fluid dynamic to achieve more accurate and reliable results as well as the microfluidic MFC structures' evaluation on microbial behaviors by experimental investigations are suggested to outline further researches.

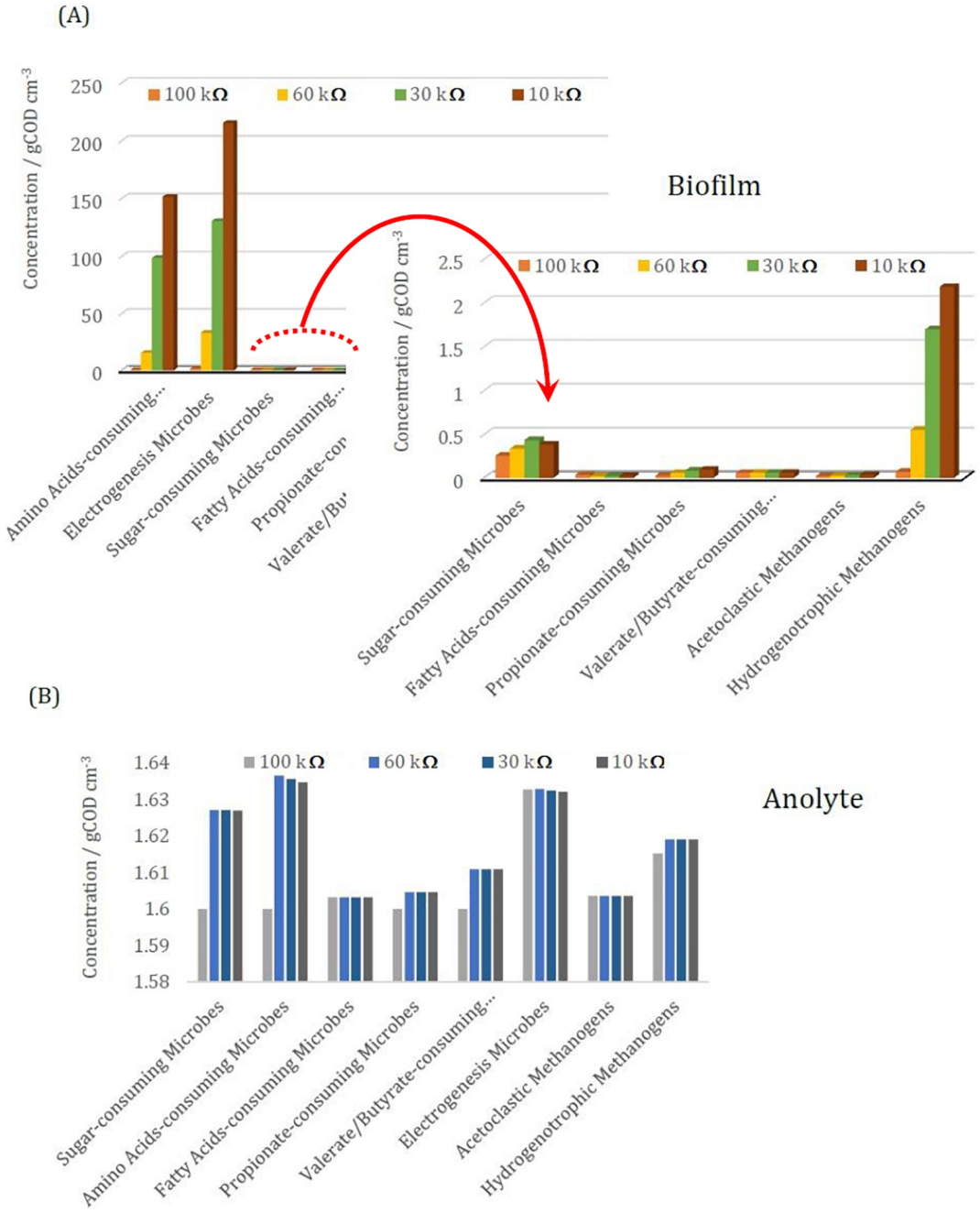

Fig. 7. Influence of external resistance on sustained concentration of each microbial group in (A) biofilm and (B) anolyte. The microchannel diameter, substrate flow rate and external resistance range were 1000 μm,100 μl h^{-1} and 10 to 100 kΩ, respectively.

Acknowledgments

This research was supported by Vice President for Research, Sharif University of Technology, under grant number QA 970713.

Appendix A. Supplementary data

Supplementary data to this article can be found online at https://doi.org/10.1016/j.bioelechem.2019.03.003.

References

[1] S. Goel, From waste to watts in micro-devices: review on development of membraned and membraneless microfluidic microbial fuel cell, Appl. Mater. Today 11 (2018) 270–279.
[2] Y. Yang, D. Ye, J. Li, X. Zhu, Q. Liao, B. Zhang, Microfluidic microbial fuel cells: from membrane to membrane free, J. Power Sources 324 (2016) 113–125.
[3] H.-Y. Wang, A. Bernarda, C.-Y. Huang, D.-J. Lee, J.-S. Chang, Micro-sized microbial fuel cell: a mini-review, Bioresour. Technol. 102 (2011) 235–243.
[4] K.B. Lam, E.A. Johnson, M. Chiao, L. Lin, A MEMS photosynthetic electrochemical cell powered by subcellular plant photosystems, J. Microelectromech. S. 15 (2006) 1243–1250.
[5] Y.-P. Chen, Y. Zhao, K.-Q. Qiu, J. Chu, R. Lu, M. Sun, X.-W. Liu, G.-P. Sheng, H.-Q. Yu, J. Chen, An innovative miniature microbial fuel cell fabricated using photolithography, Biosens. Bioelectron. 26 (2011) 2841–2846.
[6] J.Y. Yoon, Y. Ahn, U. Schröder, Parylene C-coated PDMS-based microfluidic microbial fuel cells with low oxygen permeability, J. Power Sources 398 (2018) 209–214.
[7] Y. Jiang, X. Yang, P. Liang, P. Liu, X. Huang, Microbial fuel cell sensors for water quality early warning systems: fundamentals, signal resolution, optimization and future challenges, Renew. Sust. Energ. Rev. 81 (2018) 292–305.
[8] D. Wang, P. Liang, Y. Jiang, P. Liu, B. Miao, W. Hao, X. Huang, Open external circuit for microbial fuel cell sensor to monitor the nitrate in aquatic environment, Biosens. Bioelectron. 111 (2018) 97–101.

[9] Y. Zhang, I. Angelidaki, A simple and rapid method for monitoring dissolved oxygen in water with a submersible microbial fuel cell (SBMFC), Biosens. Bioelectron. 38 (2012) 189–194.
[10] Y. Zhang, I. Angelidaki, Submersible microbial fuel cell sensor for monitoring microbial activity and BOD in groundwater: focusing on impact of anodic biofilm on sensor applicability, Biotechnol. Bioeng. 108 (2011) 2339–2347.
[11] M. Asghary, J.B. Raoof, M. Rahimnejad, R. Ojani, A novel self-powered and sensitive label-free DNA biosensor in microbial fuel cell, Biosens. Bioelectron. 82 (2016) 173–176.
[12] X. Jin, I. Angelidaki, Y. Zhang, Microbial electrochemical monitoring of volatile fatty acids during anaerobic digestion, Environ. Sci. Technol. 50 (2016) 4422–4429.
[13] X. Jin, X. Li, N. Zhao, I. Angelidaki, Y. Zhang, Bio-electrolytic sensor for rapid monitoring of volatile fatty acids in anaerobic digestion process, Water Res. 111 (2017) 74–80.
[14] A. Schievano, A. Colombo, A. Cossettini, A. Goglio, V. D'Ardes, S. Trasatti, P. Cristiani, Single-chamber microbial fuel cells as on-line shock-sensors for volatile fatty acids in anaerobic digesters, Waste Manag. 71 (2018) 785–791.
[15] W.-F. Cai, J.-F. Geng, K.-B. Pu, Q. Ma, D.-W. Jing, Y.-H. Wang, Q.-Y. Chen, H. Liu, Investigation of a two-dimensional model on microbial fuel cell with different biofilm porosities and external resistances, Chem. Eng. J. 333 (2018) 572–582.
[16] V.M. Ortiz-Martínez, M.J. Salar-García, A.P. de los Ríos, F.J. Hernández-Fernández, J.A. Egea, L.J. Lozano, Developments in microbial fuel cell modeling, Chem. Eng. J. 271 (2015) 50–60.
[17] C. Xia, D. Zhang, W. Pedrycz, Y. Zhu, Y. Guo, Models for microbial fuel cells: a critical review, J. Power Sources 373 (2018) 119–131.
[18] H.-Y. Wang, J.-Y. Su, Membraneless microfluidic microbial fuel cell for rapid detection of electrochemical activity of microorganism, Bioresour. Technol. 145 (2013) 271–274.
[19] P. Parkhey, S.V. Mohan, Biosensing Applications of Microbial Fuel Cell: approach toward Miniaturization, Microbial Electrochemical Technology, Elsevier, 2019 977–997.
[20] S. Ou, H. Kashima, D.S. Aaron, J.M. Regan, M.M. Mench, Multi-variable mathematical models for the air-cathode microbial fuel cell system, J. Power Sources 314 (2016) 49–57.
[21] C. Santoro, C. Arbizzani, B. Erable, I. Ieropoulos, Microbial fuel cells: from fundamentals to applications. A review, J. Power Sources 356 (2017) 225–244.
[22] H. Jia, G. Yang, H.-H. Ngo, W. Guo, H. Zhang, F. Gao, J. Wang, Enhancing simultaneous response and amplification of biosensor in microbial fuel cell-based upflow anaerobic sludge bed reactor supplemented with zero-valent iron, Chem. Eng. J. 327 (2017) 1117–1127.
[23] Y. Xiao, C. De Araujo, C.C. Sze, D.C. Stuckey, Toxicity measurement in biological wastewater treatment processes: a review, J. Hazard. Mater. 286 (2015) 15–29.
[24] D.J. Batstone, J. Keller, I. Angelidaki, S.V. Kalyuzhnyi, S.G. Pavlostathis, A. Rozzi, W.T.M. Sanders, H. Siegrist, V.A. Vavilin, The IWA anaerobic digestion model no 1 (ADM1), Water Sci. Technol. 45 (2002) 65–73.
[25] M.K. Alavijeh, M.M. Mardanpour, S. Yaghmaei, One-dimensional conduction-based Modeling of bioenergy production in a microbial fuel cell engaged with multi-population biocatalysts, Electrochim. Acta 184 (2015) 151–163.
[26] R. Pinto, B. Srinivasan, A. Escapa, B. Tartakovsky, Multi-population model of a microbial electrolysis cell, Environ. Sci. Technol. 45 (2011) 5039–5046.
[27] M.M. Mardanpour, S. Yaghmaei, Characterization of a microfluidic microbial fuel cell as a power generator based on a nickel electrode, Biosens. Bioelectron. 79 (2016) 327–333.
[28] M.M. Mardanpour, S. Yaghmaei, M. Kalantar, Modeling of microfluidic microbial fuel cells using quantitative bacterial transport parameters, J. Power Sources 342 (2017) 1017–1031.
[29] F. Yu, N.D.S. Kumar, D. Choudhury, L.C. Foo, S.H. Ng, Microfluidic platforms for modeling biological barriers in the circulatory system, Drug discov. today 23 (4) (2018) 815–829.
[30] F. El Moustaid, A. Eladdadi, L. Uys, Modeling bacterial attachment to surfaces as an early stage of biofilm development, Math. Biosci. Eng. 10 (2013) 821–842.
[31] M.J. Tindall, P.K. Maini, S.L. Porter, J.P. Armitage, Overview of mathematical approaches used to model bacterial chemotaxis II: bacterial populations, Bull. Math. Biol. 70 (2008) 1570–1607.
[32] E.F. Keller, L.A. Segel, Traveling bands of chemotactic bacteria: a theoretical analysis, J. Theor. Biol. 30 (1971) 235–248.
[33] Y.A. Gorby, S. Yanina, J.S. McLean, K.M. Rosso, D. Moyles, A. Dohnalkova, T.J. Beveridge, I.S. Chang, B.H. Kim, K.S. Kim, Electrically conductive bacterial nanowires produced by Shewanella oneidensis strain MR-1 and other microorganisms, Proc. Natl. Acad. Sci. 103 (2006) 11358–11363.
[34] U. Schröder, Anodic electron transfer mechanisms in microbial fuel cells and their energy efficiency, Phys. Chem. Chem. Phys. 9 (2007) 2619–2629.
[35] A. Kato Marcus, C.I. Torres, B.E. Rittmann, Conduction-based modeling of the biofilm anode of a microbial fuel cell, Biotechnol. Bioeng. 98 (2007) 1171–1182.
[36] P. Kuntke, K. Śmiech, H. Bruning, G. Zeeman, M. Saakes, T. Sleutels, H. Hamelers, C. Buisman, Ammonium recovery and energy production from urine by a microbial fuel cell, Water Res. 46 (2012) 2627–2636.
[37] M.K. Alavijeh, M.M. Mardanpour, S. Yaghmaei, A generalized model for complex wastewater treatment with simultaneous bioenergy production using the microbial electrochemical cell, Electrochim. Acta 167 (2015) 84–96.
[38] F.X. Kelly, K.J. Dapsis, D.A. Lauffenburger, Effect of bacterial chemotaxis on dynamics of microbial competition, Microb. Ecol. 16 (1988) 115–131.
[39] M.K. Alavijeh, S. Yaghmaei, M.M. Mardanpour, A combined model for large scale batch culture MFC-digester with various wastewaters through different populations, Bioelectrochemistry 106 ((2015) 298–307.
[40] L. Zhang, X. Zhu, J. Li, Q. Liao, D. Ye, Biofilm formation and electricity generation of a microbial fuel cell started up under different external resistances, J. Power Sources 196 (2011) 6029–6035.
[41] M.M. Mardanpour, M.N. Esfahany, T. Behzad, R. Sedaqatvand, Single chamber microbial fuel cell with spiral anode for dairy wastewater treatment, Biosens. Bioelectron. 38 (2012) 264–269.
[42] M. Hasany, M.M. Mardanpour, S. Yaghmaei, Biocatalysts in microbial electrolysis cells: a review, Int. J. Hydrog. Energy 41 (2016) 1477–1493.
[43] J. Wang, L. Ding, K. Li, H. Huang, H. Hu, J. Geng, K. Xu, H. Ren, Estimation of spatial distribution of quorum sensing signaling in sequencing batch biofilm reactor (SBBR) biofilms, Sci. Total Environ. 612 (2018) 405–414.